EUROFUSION WP14ER-PR(14) 12701

P Tolias et al.

Dust remobilization in fusion plasmas

Preprint of Paper to be submitted for publication in
Nuclear Fusion

This work has been carried out within the framework of the EUROfusion Consortium and has received funding from the Euratom research and training programme 2014-2018 under grant agreement No 633053. The views and opinions expressed herein do not necessarily reflect those of the European Commission.

Dust remobilization in fusion plasmas

P. Tolias,[1] S. Ratynskaia,[1] M. De Angeli,[2] G. De Temmerman,[3] D. Ripamonti,[4] G. Riva,[4] I. Bykov,[1] A. Shalpegin,[5,6] L. Vignitchouk,[1] F. Brochard,[5] K. Bystrov,[7] S. Bardin,[7] and A. Litnovsky[8]

[1]KTH Royal Institute of Technology, Association EUROfusion-VR, Stockholm, Sweden
[2]Istituto di Fisica del Plasma - Consiglio Nazionale delle Ricerche, Milan, Italy
[3]ITER Organization, Route de Vinon-sur-Verdon, CS 90 046, 13067 St-Paul-Lez-Durance Cedex, France
[4]Istituto per l'Energetica e le Interfasi - Consiglio Nazionale delle Ricerche, Milan, Italy
[5]Université de Lorraine, Institut Jean Lamour, Vandoeuvre-lés-Nancy, France
[6]IGVP, Universität Stuttgart, Stuttgart, Germany
[7]FOM Institute DIFFER, Dutch Institute For Fundamental Energy Research, Nieuwegein, The Netherlands
[8]Institute of Energy and Climate Research - Plasma Physics, Forschungszentrum Jülich, Jülich, Germany

E-mail: panagiotis.tolias@ee.kth.se

Abstract. The first combined experimental and theoretical studies of dust remobilization by plasma forces are reported. The main theoretical aspects of remobilization are analyzed. In particular, the role of adhesive forces is highlighted and generic remobilization conditions are formulated. A novel experimental technique is proposed, based on controlled adhesion of dust grains on tungsten samples combined with detailed mapping of the dust deposition profile prior and post plasma exposure. Proof-of-principle experiments in the TEXTOR tokamak and the EXTRAP-T2R reversed-field pinch are presented. The versatile environment of the linear device Pilot-PSI allowed for experiments with different magnetic field topologies and varying plasma conditions that were complemented with camera observations.

1. Introduction

It has been long realised that dust remobilization is a major safety issue for ITER and future fusion devices, owing to the possibility of radioactive or toxic dust release upon loss of vacuum accidents (LOVAs) [1, 2, 3]. In such scenarios, air ingress in the vacuum vessel creates an outward flow after pressure equilibration which leads to hydrodynamic forces that can potentially mobilize dust grains [4, 5]. Moreover, dust remobilization upon disruptions has been consistently observed in multiple tokamaks by cameras [6, 7, 8, 9, 10] and other diagnostics [10, 11]. In such cases, vibrations of plasma-facing components (PFCs), thermal shocks [12] or large currents induced by fast transients most probably provide the mobilizing forces. Finally, dust can also be remobilized in normal operating conditions by plasma forces. Regardless of the scenario, remobilization is a consequence of momentum imbalance in the "dust-PFC contact". Hence, the main differentiating factor between remobilization in LOVAs, disruptions and normal operating conditions is the mobilizing force or torque.

Deeper understanding of the mechanism of remobilization by plasma forces can play an important role in diverse plasma-wall interaction issues: *Specification of realistic initial conditions for the ejection speed and angle of remobilized dust grains.* This will increase the predictive power of dust transport codes as far as the grain penetration depth and the amount of dust-associated impurities are concerned. Consequently, this can lead to a more accurate modelling of transient impurity events [13, 14], intense radiation spikes most likely associated with mobile dust re-distributed by a temporally adjacent disruptive discharge [15]. *Specification of realistic dust trajectory termination conditions.* So far, MIGRAINe is the only code that treats dust-wall interactions [16, 17, 18] and thus has the potential to make predictions with respect to the in-vessel sites where dust will most likely accumulate. However, in the current version of MIGRAINe [17], dust trajectories terminate for impacts that satisfy the sticking condition since remobilization is not accounted for. We stress that identification of preferred dust accumulation sites is the first step in developing efficient *in situ* dust removal techniques. For instance, in ITER, mechanical dust removal is envisaged and hence successful predictions of the location of such sites can lead to dust collection by the divertor remote handling system or the multi-purpose deployment system [19]. *Quantification of dust amassment in the grooves of castellated PFCs.* In ITER, PFCs will be castellated, i.e. split into small segments separated by thin gaps [20, 21]. The gap entrance corresponds to a small fraction of the plasma-exposed area (the gap width is 0.5 mm), implying that dust trajectories directly terminating in the gaps can be considered rare. Two mechanisms related with the physics of the dust-PFC contact can be more efficient: dust remobilization from neighbouring monoblocks (provided that the release velocity is nearly tangential and low enough to ensure that the motion is governed not only by inertia but also by potential effects) or dust impacting and subsequently rolling or sliding on neighbouring monoblocks. *Evaluation of the gap trapping efficiency.* A closely related issue concerns grains already residing in the gaps and in particular

whether they are permanently stuck therein or can be remobilized during normal plasma conditions or by a disruption.

Despite its importance, the remobilization of dust grains in normal operating conditions has not been properly considered thus far. There are no relevant experimental results, whereas previous theoretical investigations have either erroneously neglected the role of adhesion [22, 23, 24, 25] or adopted an oversimplifying description of the phenomenon [12]. In this work, we carry out the first combined experimental and theoretical study of dust remobilization in fusion plasmas during normal operating conditions. The main theoretical aspects of remobilization are analyzed, the role of adhesion in both establishing and breaking the dust-PFC contact is highlighted, whereas generic remobilization conditions are formulated. An experimental technique is proposed based on controlled pre-adhesion of dust grains on samples and detailed mapping of the deposition profiles prior to and post plasma exposure. Such a technique realistically mimics naturally occurring remobilization. Proof-of-principle of the technique is provided by experiments with planar tungsten samples in the TEXTOR tokamak and the EXTRAP-T2R reversed-field pinch. It is shown that plasma forces are sufficient to remobilize the grain and first quantitative estimates of the remobilization activity are performed. Further experiments in the Pilot-PSI linear device enabled studies under varying plasma conditions and magnetic field topology. They were complemented by camera observations allowing for estimates of the ejection speed and angle.

2. Theoretical aspects of dust remobilization in fusion plasmas

2.1. The sticking impact regime

Before delving into the physics of remobilization, it is essential to discuss how dust gets originally stuck on plasma facing components. This is a crucial design element of controlled remobilization experiments, since, in order to allow for reliable extrapolations, dust grain deposition on samples needs to mimic dust sticking on PFCs as it naturally occurs in fusion environments. For a dust grain impinging obliquely on a smooth surface, when the normal impact velocity is smaller than a critical value known as the sticking velocity v_{s}, all the normal kinetic energy of the grain is dissipated into adhesive work and plastic deformation. Consequently, the rebound velocity will be purely tangential and, in absence of strong external forces, it will slowly decrease owing to kinetic friction, until the dust grain is completely immobilized.

During the dust-PFC collision, the work carried out by external plasma forces is negligible compared to the impact energy of the grain and the total interface energy, *i.e.* the work necessary to separate the two surfaces from contact to infinity. As we shall see in the following subsection, not only the work but also the normal component of the external forces themselves is negligible. This opens up the way for a treatment of dust-PFC collisions with established impact mechanics models [26]. An analytical model of the normal component of elastic-perfectly plastic adhesive impacts originally developed

by Thornton and Ning (T&N model) [27] has proved to be successful in reproducing experimental data [28] and has been recently incorporated in the MIGRAINe dust dynamics code [16, 17, 18]. In the T&N model, sticking is essentially controlled by two characteristic velocities, the adhesive velocity associated with adhesive work and the yield velocity associated with plastic work.

The *adhesive velocity* is the maximum impact velocity for which an elastic-adhesive impact leads to zero rebound velocity. For such impacts, sticking is a consequence of the irreversible work of microscopic attractive inter-particle forces. Therefore, the adhesive velocity can be found by equating the normal impact kinetic energy of the grain with the total inelastic work carried out throughout the impact, from the initiation of the contact up to the separation of the surfaces of the colliding bodies. It naturally depends on the adhesive theory employed. Within the Johnson-Kendall-Roberts theory [29], that is assumed in the T&N model, it is given by

$$v_{\rm s}^{\rm adh} = \frac{\sqrt{3}}{2}\pi^{1/3}\sqrt{\frac{1+6\times 2^{2/3}}{5}}\left(\frac{\Gamma^5}{\rho_{\rm d}^3 E^{*2} R_{\rm d}^5}\right)^{1/6}, \tag{1}$$

where Γ is the interface energy per unit area, $\rho_{\rm d}$ is the dust mass density, $R_{\rm d}$ is the dust radius and E^* is the reduced Young modulus. The size dependence of the adhesive velocity is explicit.

The *yield velocity* is the minimum impact velocity for which a pure elastic impact starts to become plastic. For the onset of plastic deformation beneath the contact region, the pressure at any point needs to exceed a limiting contact pressure $p_{\rm y}$ that is proportional to the yield strength $\sigma_{\rm y}$ of the material. For Hertzian profiles the maximum of the pressure is attained at the center of the contact area and the above criterion leads to a limiting contact radius $a_{\rm y} = (\pi R_{\rm d} p_{\rm y}) / (2E^*)$. Therefore, the yield velocity can be found by equating the normal impact kinetic energy of the grain with the elastic energy stored in the contact $U_{\rm el}(\delta_{\rm y})$ at a penetration depth $\delta_{\rm y} = a_{\rm c}^2/R_{\rm d}$. This leads to the expression

$$v_{\rm y} = \frac{\pi^2}{2\sqrt{10}}\left(\frac{p_{\rm y}^5}{\rho_{\rm d} E^{*4}}\right)^{1/2}. \tag{2}$$

There is an implicit size dependence that is incorporated in $p_{\rm y}$. Material properties and especially the yield strength strongly depend not only on the bulk dust temperature $T_{\rm d}$ but also on the dust size. In fact, as far as the onset of plastic deformation is concerned, there is a competition between the enhanced plasticity of heated metals and the high yield strength of micrometer-scale bodies. The $\Gamma(T_{\rm d})\,, \rho_{\rm d}(T_{\rm d})\,, E^*(T_{\rm d})$ and $\sigma_{\rm y}(T_{\rm d}, R_{\rm d})$ dependencies for tungsten and beryllium have been described in Ref. [17].

Based on the value of these characteristic velocities, two distinct sticking realizations emerge. When $v_{\rm y} \geq v_{\rm s}^{\rm adh}$, plastic deformation does not occur during sticking impacts and the sticking velocity is equal to the adhesive velocity, $v_{\rm s} = v_{\rm s}^{\rm adh}$. On the other hand, when $v_{\rm y} < v_{\rm s}^{\rm adh}$, plastic work affects sticking and the sticking velocity is larger than the adhesive velocity, $v_{\rm s} > v_{\rm s}^{\rm adh}$. In order to distinguish between the two sticking realizations, it is convenient to define the dust threshold radius $R_{\rm d}^{\rm th}(T_{\rm d})$ that corresponds to the dust

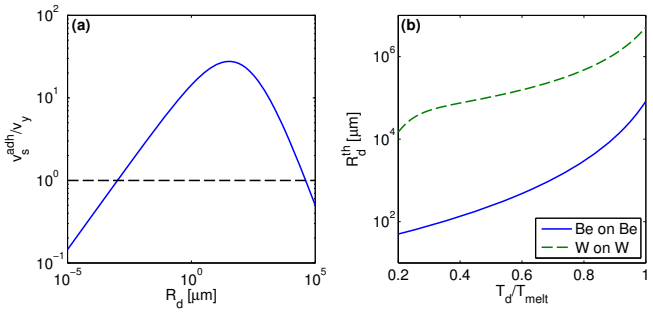

Figure 1. (a) The ratio of the adhesive velocity to the yield velocity for W on W impact and $T_{\rm d} = 1000\,K$. Notice that two solutions of the equation $v_{\rm y}(R_{\rm d}) = v_{\rm s}^{\rm adh}(R_{\rm d})$ exist. For dust grains with radii that belong to the interval between the two solutions, $v_{\rm y} < v_{\rm s}^{\rm adh}$ and plastic deformation affects sticking. (b) Plot of the dust threshold radius as a function of the dust bulk temperature. For W dust impinging on W samples $R_{\rm d}^{\rm th} > 10\,$mm for any temperature, while for Be dust impinging on Be samples $R_{\rm d}^{\rm th} \gg 10\,\mu$m.

size for which the adhesive velocity and the yield velocity are equal. In Ref. [16], the dependence of mechanical properties on $(T_{\rm d}\,, R_{\rm d})$ was not taken into account, which led to a single value of the dust threshold radius. Including these dependencies, we observe that for each value of the bulk dust temperature there exist two solutions of the equation $v_{\rm y}(R_{\rm d}) = v_{\rm s}^{\rm adh}(R_{\rm d})$, see figure 1(a). The smaller solution is of no interest since it always lies in the nanometer scale; it is a manifestation of the Hall-Petch strengthening effect and demonstrates that for nano-sized dust plastic deformation is difficult to induce. Therefore, we shall identify the larger solution as the dust threshold radius $R_{\rm d}^{\rm th}(T_{\rm d})$: for $R_{\rm d} > R_{\rm d}^{\rm th}(T_{\rm d})$ plastic deformation has no effect in sticking.

The threshold radius is plotted in figure 1(b) as a function of the dust bulk temperature for W on W impacts and Be on Be impacts. We conclude that plastic deformation is always important for tokamak relevant impacts. Owing to the dependence of plastic deformation on the impact energy, after the dust grain is immobilized, the details of the contact region will also depend on the normal component of the grain impact velocity. This dependence on the pre-history of the trajectory clearly implies that control of the impact velocity prior to sticking should be an essential ingredient of reliable remobilization experiments.

2.2. Simple estimates of the role of adhesion on remobilization

In this subsection, we shall focus on the adhesive forces acting on the contact area that is established between the dust grain and the PFC after an impact in the sticking regime. For simplicity, we assume perfectly smooth surfaces and neglect plasticity. Plastic deformation will increase the contact area and thus the net adhesive force. We shall analyze the elastic-adhesive contact with the aid of macroscopic contact mechanics.

We introduce the Hertzian elastic energy $U_{\rm el}$, the contact radius a and the Hertzian penetration depth $\delta = a^2/R_{\rm d}$. A heuristic approach due to Derjaguin assumes the

validity of the Hertzian elastic contact equations and simply includes adhesion as a negative energy contribution [30], which is approximated by $-\pi a^2\Gamma$. Therefore, the total energy of the system will be $U(\delta) = U_{\rm el}(\delta) - \pi a^2\Gamma$ and the contact force applied to the grain will be given by $F_{\rm c}(\delta) = \partial U/\partial\delta = F_{\rm el}(\delta) - \pi R_{\rm d}\Gamma$. Pull-off is achieved at $\delta = a = 0$ and the pull-off force, *i.e.* the minimum external normal force required to separate the surfaces, is given by $F_{\rm po} = \pi R_{\rm d}\Gamma$. Despite its simplicity, this heuristic model is useful for order of magnitude estimates. In fact, in more elaborate theories of elastic-adhesive contact, the pull-off force always has the form

$$F_{\rm po} = \xi_{\rm a}\pi R_{\rm d}\Gamma\,, \tag{3}$$

with $\xi_{\rm a}$ a dimensionless coefficient of the order of a few [31]. For instance, in the Johnson-Kendall-Roberts theory $\xi_{\rm a} = 3/2$ [29], whereas in the Derjaguin-Muller-Toporov theory $\xi_{\rm a} = 2$ [32].

The proportionality of the pull-off force with the dust radius is indicative of the dominant role of adhesion for micron-sized grains, since other forces acting on grains embedded in fusion devices scale either as $R_{\rm d}^2$ or as $R_{\rm d}^3$. A similar proportionality also stems from microscopic descriptions of the contact. Within the DLVO theory [33], the total interaction between any two surfaces can be decomposed into the net Van der Waals force, as calculated with the additivity approach of Hamaker, and the electric double-layer force. For a sphere in contact with a flat surface, both the forces are proportional to the radius of the sphere [34]. Let us now compare the pull-off force with the main external forces.

For a homogeneous infinite Maxwellian flowing plasma, the drag force due to the scattering of hydrogenic ions is given by [35]

$$F_{\rm id}^{\rm sc} = 2\sqrt{2\pi}R_{\rm d}^2 m_{\rm i} n_{\rm i} v_{\rm Ti} v_{\rm i} (z^2/\tau_{\rm i}^2) \ln(\Lambda_{\rm i}) \mathcal{G}(u_{\rm i})\,, \tag{4}$$

where $v_{\rm Ti} = \sqrt{T_{\rm i}/m_{\rm i}}$ is the ion thermal velocity, $v_{\rm i}$ is the ion flow, $z = -e\phi_{\rm d}/T_{\rm e}$ is the normalized dust potential, $\tau_{\rm i} = T_{\rm i}/T_{\rm e}$ is the ion-to-electron temperature ratio, $\ln(\Lambda_{\rm i})$ is the effective Coulomb logarithm, $u_{\rm i} = v_{\rm i}/\sqrt{2}v_{\rm Ti}$ and $\mathcal{G}(u) = [\sqrt{\pi}{\rm erf}(u) - 2ue^{-u^2}]/(2u^3)$. Similarly, for the drag force due to absorption of hydrogenic ions we have $F_{\rm id}^{\rm abs} \propto R_{\rm d}^2$. Owing to the strong plasma inhomogeneity in the sheath and the effect of the boundary in binary collisions, the ion drag force expression is not valid and the force due to momentum exchange with ions will also possess a lift component, *i.e.* a component perpendicular to the direction of the ion flow.

For a perfectly spherical conducting grain lying on a conducting plane in the presence of a uniform normal electric field $E_{\rm w}$, the boundary value problem for the determination of the electrostatic potential has an analytical solution [36]. For this configuration, the contact charge of dust is given by $Q_{\rm d} = -\zeta(2)R_{\rm d}^2 E_{\rm w} \simeq -1.64R_{\rm d}^2 E_{\rm w}$ and the normal electrostatic force acting on the grain is given by the formula $F_{\rm E} = [1/6 + \zeta(3)]\, R_{\rm d}^2 E_{\rm w}^2$ or equivalently

$$F_{\rm E} = 1.37 R_{\rm d}^2 E_{\rm w}^2\,, \tag{5}$$

where $\zeta(.)$ denotes Riemann's zeta-function. The electrostatic force expression stems from the solution of the Laplace equation with one of the boundary conditions resulting from the constant behavior of the electric field at infinity. Thus, it is clearly not valid in our case. However, both Eq.(4) and Eq.(5) are convenient for our purposes, since they are expected to significantly overestimate the forces involved. Finally, denoting with g the gravitational acceleration, the gravitational force is given by $F_{\mathrm{g}} = \frac{4}{3}\pi R_{\mathrm{d}}^3 \rho_{\mathrm{d}} g$.

In the parameter range relevant to ITER divertor conditions, selecting favorable plasma conditions for the ion drag and electrostatic forces to be large ($n_{\mathrm{e}} = 10^{14}\,\mathrm{cm}^{-3}$, $T_{\mathrm{e}} = T_{\mathrm{i}} = 10\,\mathrm{eV}$, $z = 3$, $v_{\mathrm{i}} = \sqrt{2} v_{\mathrm{Ti}}$, $E_{\mathrm{w}} = 30\,\mathrm{kV/cm}$) and assuming relatively large tungsten dust of 10 micron diameter, we have

$$F_{\mathrm{po}} \sim 10^2 F_{\mathrm{id}}^{\mathrm{sc}} \sim 10^3 F_{\mathrm{id}}^{\mathrm{abs}} \sim 10^3 F_E \sim 10^6 F_{\mathrm{g}} \,. \tag{6}$$

Even when accounting for the effect of nano-scale roughness, which will inevitably decrease adhesion [37], it is apparent that the pull-off force is orders of magnitude larger than the plasma forces and gravity. Therefore, previous investigations of dust remobilization that neglected adhesion are unrealistic [22, 23, 24, 25].

2.3. Forces exerted on a dust grain in contact with the PFC

In our discussion of the sticking impact regime, we neglected the effect of plasma forces based on energy budget arguments. Whereas in the previous subsection, we demonstrated that the pull-off force is orders of magnitude larger than plasma forces. However, plasma forces need to be responsible for remobilization, being essentially the only external forces exerted on the grain. In the formulation of remobilization conditions, due to the static nature of the problem, we can greatly benefit from the use of force diagrams. The forces on a dust grain that is stuck on the PFC are sketched in figure 2. We neglect the gravitational force, since it is orders of magnitude smaller than the other forces.

A first class of forces originates from the interaction of the dust grain with the plasma. As aforementioned, owing to the ion flow direction not being an axis of symmetry and the strong inhomogeneity of the sheath, the interaction with the plasma ions results in both drag and lift components. As a consequence, a tangential force $\boldsymbol{F}_{\mathrm{i}}^{\mathrm{t}}$ is exerted to the grain due to the scattering and absorption of ions that can be decomposed into the ion drag force due to the tangential component of the ion flow $\boldsymbol{F}_{\mathrm{id}}^{\mathrm{t}}$ and the ion lift force due to the normal component of the ion flow $\boldsymbol{F}_{\mathrm{iL}}^{\mathrm{t}}$, with $\boldsymbol{F}_{\mathrm{i}}^{\mathrm{t}} = \boldsymbol{F}_{\mathrm{id}}^{\mathrm{t}} + \boldsymbol{F}_{\mathrm{iL}}^{\mathrm{t}}$. A normal force $\boldsymbol{F}_{\mathrm{i}}^{\mathrm{n}}$ is also exerted to the grain due to momentum exchange with the plasma ions. In a similar fashion, it can be decomposed into the ion drag force due to the normal component of the ion flow $\boldsymbol{F}_{\mathrm{id}}^{\mathrm{n}}$ and the ion lift force due to the tangential component of the ion flow $\boldsymbol{F}_{\mathrm{iL}}^{\mathrm{n}}$, with $\boldsymbol{F}_{\mathrm{i}}^{\mathrm{n}} = \boldsymbol{F}_{\mathrm{id}}^{\mathrm{n}} + \boldsymbol{F}_{\mathrm{iL}}^{\mathrm{n}}$. The forces $\boldsymbol{F}_{\mathrm{i}}^{\mathrm{t}}$ and $\boldsymbol{F}_{\mathrm{i}}^{\mathrm{n}}$ can be assumed to have lines of action traversing the center of mass of the grain, provided that the excess torque is compensated for by the so-called external moment of surface stresses about the center, denoted here by $\boldsymbol{M}_{\mathrm{i}}$ [38, 39]. Finally, there is an electrostatic force

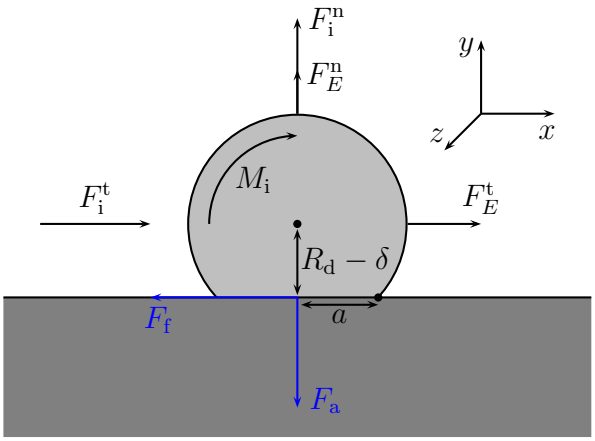

Figure 2. Force diagram of a dust grain in contact with the PFC (the plasma forces carry a sign). Both surfaces are assumed to be perfectly smooth, for simplicity it is also assumed that $\boldsymbol{F}_{\rm i}^{\rm t} \| \boldsymbol{F}_{\rm E}^{\rm t}$.

$\boldsymbol{F}_{\rm E} = \boldsymbol{F}_{\rm E}^{\rm n} + \boldsymbol{F}_{\rm E}^{\rm t}$ acting on the dust grain due to the electrostatic field of the surrounding plasma sheath.

A second class of forces originates from the contact between the dust grain and the wall. In the normal direction, adhesive forces $\boldsymbol{F}_{\rm a}$ are exerted. They resist any external forces tending to separate the contact between the bodies. The minimum external force necessary to separate the two surfaces is the pull-off force $\boldsymbol{F}_{\rm po}$. In the tangential direction, frictional forces $\boldsymbol{F}_{\rm f}$ are exerted. They resist any external forces inducing relative motion between the bodies in contact. The maximum of the net frictional force, or equivalently the minimum external force necessary to cause sliding between the bodies is the static friction $\boldsymbol{F}_{\rm fs}$. We assume the validity of Amontons's law $F_{\rm fs} = \mu_{\rm s} F_{\rm N}$, with $\mu_{\rm s}$ the coefficient of static friction and $F_{\rm N}$ the normal component of the total force. It might seem contradictory to the reader that, even though we assume that both the dust grain and the wall are smooth surfaces, the coefficient of static friction is considered non-zero. In fact, in traditional theories [40], static friction is the consequence of surface asperity interlocking and arises from the dissipative processes that accompany the engagement / disengagement of micro-asperities. Such a picture is outdated [41, 42] and it has been experimentally demonstrated that even smooth surfaces can exhibit strong friction owing to atomic forces and local deformation processes. We note that, also in microscopic theories, static friction preserves its proportionality with the normal component of the force, in accordance with Amontons's law [43].

2.4. Generic remobilization conditions

Assuming for simplicity that $\boldsymbol{F}_{\rm i}^{\rm t} \| \boldsymbol{F}_{\rm E}^{\rm t}$, the remobilization conditions can be found from force balance in the normal direction, force balance in the tangential direction and torque

balance around the contact point [44, 45, 46]:

$$\begin{aligned}
&\underline{\textit{detachment}} : F_{\rm i}^{\rm n} + F_{\rm E}^{\rm n} > F_{\rm po}\,, \\
&\underline{\textit{sliding}} : F_{\rm i}^{\rm t} + F_{\rm E}^{\rm t} > \mu_{\rm s}\,(F_{\rm po} - F_{\rm i}^{\rm n} - F_{\rm E}^{\rm n})\ , \\
&\underline{\textit{rolling}} : M_{\rm i} + (F_{\rm i}^{\rm t} + F_{\rm E}^{\rm t})(R_{\rm d} - \delta) > (F_{\rm po} - F_{\rm i}^{\rm n} - F_{\rm E}^{\rm n})\,a\,.
\end{aligned}$$

Following Eq.(6), it is clear that the detachment condition cannot be easily realized in tokamaks under normal plasma conditions. On the other hand, owing to the small deformation due to adhesion ($a, \delta \ll R_{\rm d}$) the rolling condition is more easily realized. Finally, it is hard to draw any conclusions for the sliding condition due to the involvement of the coefficient of static friction, that is difficult to quantify.

Since the detachment condition is unlikely to be satisfied in tokamaks, one could conclude that dust grains will remain on the wall once they adhere to it. Nevertheless, the presence of micron-scale roughness, implies that even though the grain will initially roll or slide, it will eventually attain a velocity component normal to the local surface. We point out that the detachment and sliding conditions will be unaltered for nano-scale roughness, since it will only alter the values of the pull-off force and the static friction coefficient. However, in case roughness controls the point of rotation, the lever arms of both tangential and normal forces will change leading to a different rolling condition [46, 47].

3. Experimental technique

The remobilization experiments are realized by controlled adhesion of micron-size dust on metal samples via gas-dynamic methods, exposure of the samples to plasma, and detailed mapping of the samples before and after their exposure.

3.1. Controlled adhesion

Controlled adhesion is achieved by a modified pellet injection system that launches dust grains with a pre-defined speed towards the metal surface. See figure 3(a) for a schematic drawing of the apparatus. Dust grains are deposited at the upper face of the sabot, whose initial position lies at the bottom end of the acceleration barrel. Vacuum is set into both the upper and the lower chamber, until the opening of the air intake, which induces an air flow that accelerates the sabot with a law depending on the size of a calibrated duct. The sabot impacts on the top of the acceleration barrel and ejects the dust grains into the upper chamber. The initial time of the dust grain release is identified by an accelerometer mounted on the bottom wall of the upper chamber that monitors the impact of the sabot. Ideally, the grain trajectory is purely deterministic, deceleration is caused by gravity and the initial velocity is equal to the sabot terminal speed. The grains follow a vertical path up to the metal target and, provided that their impact speed is lower than the sticking velocity, they adhere to the target.

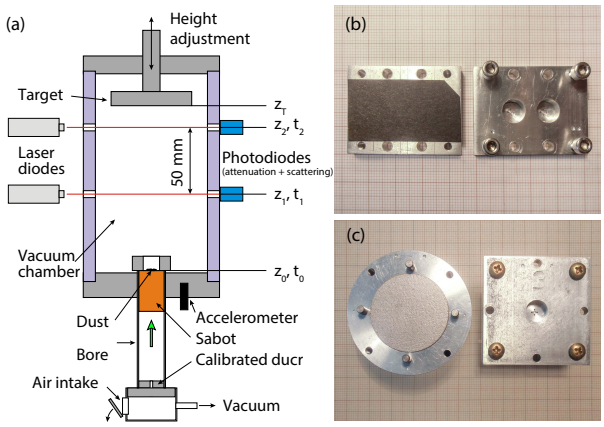

Figure 3. (a) Schematic drawing of the modified pellet injection system. (b) The sample holder and the mask for rectangular samples. (c) The sample holder and the mask for circular samples.

There are two factors that lead to uncertainties in the impact speed. Hydrodynamic forces associated with residual air in the upper chamber or with air leakages stemming from the lower chamber can slightly alter the force balance, whereas contact forces between the dust grains and the sabot can affect the initial velocity. Consequently, the dust velocity is monitored with two laser beams focused on the chamber axis. For each of the two laser diodes, three silicon-PIN-photodiodes (SIEMENS, SFH 229) are mounted on the wall, the one facing the laser diode (10^4 amplification factor) gathers the whole beam, while two additional sensors (2.1×10^7 amplification factor) are placed at $\pm 45^\circ$ from the beam direction in order to collect the scattered light. As the grains traverse the upper chamber and cross the laser beams, the attenuation of the signals is detected by the photodiodes facing the laser diodes, whereas the scattered light is detected by the other two photodiodes. The additional data provided by the second laser diode allow for a correction that accounts for grain interaction with air. We also point out that the vertical configuration of the system ensures that the grains remain immobile during the sabot acceleration.

A critical issue concerns the details of dust deposition at the sabot upper surface, which not only affect the total amount of released dust but can also lead to the undesired formation of agglomerates. This issue is of a great importance, particularly in the case of poly-disperse dust populations that include small size sub-populations of the order of $1\,\mu$m, since the latter have a strong tendency to form agglomerates when deposited on the sabot. A technique that prevents dust agglomeration is based on the use of glass spheres ($100 - 150\,\mu$m in diameter). The glass spheres are deposited on the sabot with their surface preemptively loaded with dust grains, which they release to the target upon impact. We shall refer to this technique as mediated adhesion in order to differentiate from direct adhesion. We note, though, that formation of some small dust clusters on the sample is unavoidable.

3.2. Dust deposition profile and sample mapping

In order to facilitate the pre- and post-exposure analysis of the samples and allow for an unambiguous identification of the dust spread and losses upon plasma exposure, it is convenient to confine the location of the adhered grains to well-defined spots, *i.e.* circular large dust density spots with a sharp gradient at the edge. Such a control of the dust deposition profiles is achieved by the use of specially designed holders and masks. The samples are thus encased in machined holders and held in place by masks bearing circular holes of assigned size at specified locations. Two different holder / mask types were constructed, depending on the geometry of the samples, rectangular and circular. The rectangular mask bears two groups of four 0.5 mm diameter holes, lying on a 2 mm diameter circle, see figure 3(b). The circular mask has a single central group of four 0.5 mm diameter holes, placed symmetrically with respect to the center, see figure 3(c). In both cases, the thickness of the mask is decreased to 0.5 mm in the vicinity the groups in order to favour the dust passage.

The pre-deposited samples are mapped before and after plasma exposure, by means of a scanning electron microscope (SEM) with a 150 magnification factor, adequate to resolve the smallest grains and sufficient to contain the 0.5 mm diameter dust spots in a single image. The identification of remobilized grains was based on superimposing backscattered or secondary electron images before and after plasma exposure and implementing an image processing software. In order to allow for an absolute superposition of the images, specific mechanical reference marks were added to all the samples. The remobilization activity for each sample is presented by such synthesized images with specific color coding. The remobilized dust is generally separated in three different groups; grains that were removed from their initial position and whose terminal position is not clear (coded by red), grains that appeared after plasma exposure and whose initial position is not clear (coded by green), grains that were clearly displaced after plasma exposure with both their initial and terminal positions clear (coded by yellow).

3.3. Reference samples

For all experimental campaigns, "reference" samples have been prepared. They have been treated in the same way as all other samples in terms of transportation, mounting on the device and vacuum exposure (pumping down and venting) but have not been exposed to the plasma. The reference samples are mapped before and after mounting in order to ensure that there is not any difference in the dust deposition profiles and hence that any kind of dust remobilization observed on the exposed samples is solely due to interaction with the plasma. Moreover, several tests on the strength of dust adhesion have been performed including for instance vibration in order to confirm that any accidental shaking of the sample will play no role in dust remobilization.

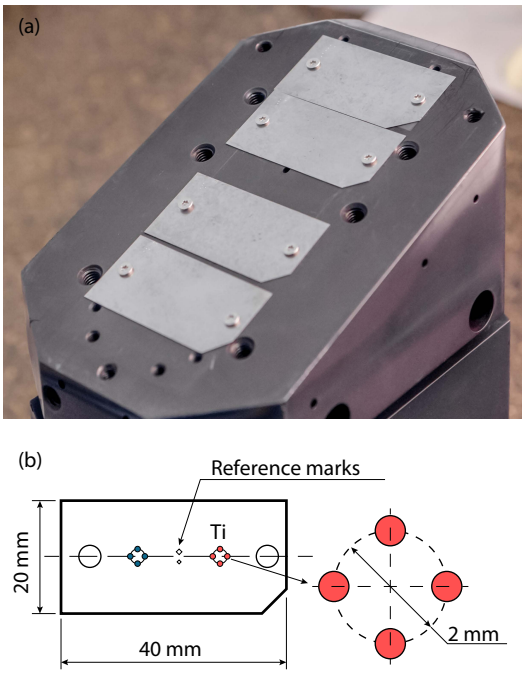

Figure 4. (a) The tungsten samples mounted on LL1. The limiter face has an inclination of 18° respect to the horizontal direction. (b) Layout of the tungsten sample and geometry of the dust spot.

4. Experimental results in fusion plasma environments

4.1. Limiter tokamak TEXTOR

Four rectangular tungsten samples were simultaneously mounted on the TEXTOR bottom limiter lock I (LLI), see figure 4(a), that was inserted at a distance $R = 52\,\mathrm{cm}$ from the torus center, *i.e.* 6 cm behind the last closed flux surface. The radial distance of the samples ranged from 52.5 to 54.7 cm. The samples were exposed to discharges #120829 and #120830 for a total of 10 s (6 s of plateau). Both discharges were NBI-heated with a total power of 1.0 MW, 2.25 T toroidal magnetic field, 350 kA plasma current and line-averaged plasma density of $3.5 \times 10^{19}\,\mathrm{m}^{-3}$.

The TEXTOR experiment involved simultaneous tungsten dust injection experiments, hence grains of different refractory materials had to be employed for an unambiguous identification of the remobilization activity. Molybdenum dust of irregular shape with a nominal dimension $< 2\,\mu$m and titanium dust of spherical shape with a nominal diameter $< 45\,\mu$m was used. The spot geometry is shown in figure 4(b), each sample contains two dust spot sets of Mo and Ti. Each set has a 2 mm diameter and comprises of four symmetrically placed spots of 0.5 mm diameter. Since Mo grains have a strong tendency to agglomerate owing to their small size and large relative surface area, their adhesion to the samples was mediated by glass spheres. On the other hand, Ti grains were directly adhered. Both the Ti spheres and the glass spheres carrying Mo

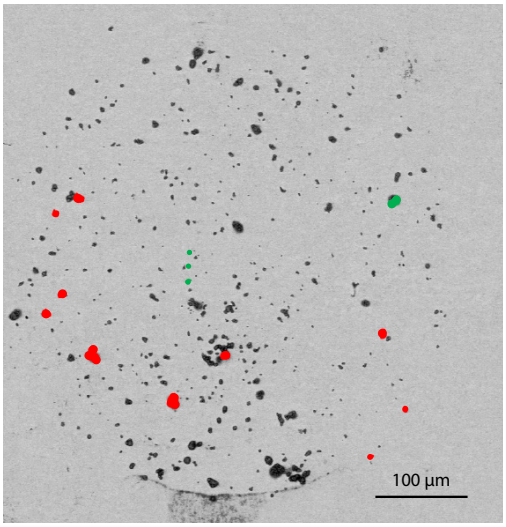

Figure 5. Synthesized backscattered electron image of a molybdenum dust spot before and after exposure to the TEXTOR plasma. Ten Mo grains were removed from the spot, four Mo grains were either displaced or originated from neighboring spots.

were deposited with an impact speed of $1 - 2\,\mathrm{m/s}$.

Analysis of the samples has provided conclusive evidence of dust remobilization under normal tokamak operation conditions. From the statistics available (total of 32 dust spots) the following picture emerges: **(i)** Spots with Mo grains underwent no changes with the exception of the sample deeper into the plasma, where some of the largest grains managed to remobilize, shown in figure 5. **(ii)** Spots with Ti grains exhibit a more intense overall remobilization activity, large grains and clusters tend to remobilize more, see figure 6 for an example of moderate activity. **(iii)** There are some instances where Ti or Mo grains are displaced from their original position without leaving the sample. Animations containing alternating SEM images of W samples prior to and post plasma exposure are provided in the online supplementary material.

4.2. Reversed-field pinch EXTRAP-T2R

In the reversed-field pinch EXTRAP-T2R [48] of major radius 1.24 m and minor radius 0.183 m, three rectangular tungsten samples were flush mounted at the flat bellow section at the outer mid plane of the device, $r = 194\,\mathrm{mm}$. See figure 1 of Ref.[49] for details of the vessel geometry. The exposure time of the samples varied from 20 ms (single dicharge) to 330 ms (multiple discharges). The discharges were not identical, the plasma current was $70 - 100\,\mathrm{kA}$, the plasma density $(0.5 - 1) \times 10^{19}\,\mathrm{m}^{-3}$ and the electron temperature in the range $100 - 200\,\mathrm{eV}$.

The sample geometry was similar to the TEXTOR experiments. Spherical tungsten dust grains TEKMAT$^{\mathrm{TM}}$ W-25 of 99.9% purity were used, supplied by "TEKNA Advanced Materials Inc" with a nominal size distribution $5 - 25\,\mu\mathrm{m}$. SEM analysis confirmed the high sphericity of the grains but revealed a small percentage of irregular

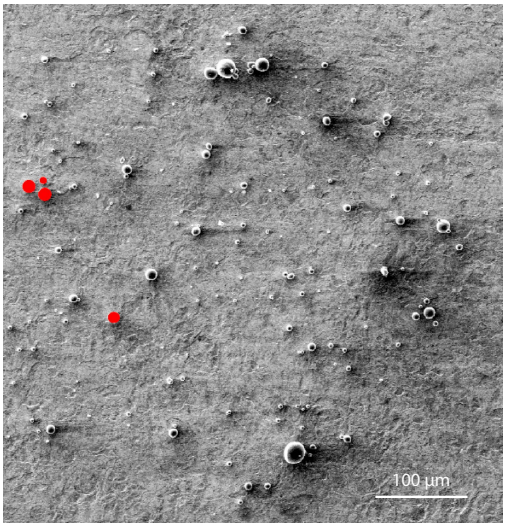

Figure 6. Synthesized secondary electron image of a titanium dust spot before and after exposure to the TEXTOR plasma. Four Ti grains were removed from the spot, three with diameter around 10 μm and one with diameter around 3 μm.

grains and the presence of a small sub-population with diameter below 5 μm. The W grains were directly adhered to the W samples with impact velocities 1.0 ± 0.1 m/s, 1.6 ± 0.1 m/s and 1.7 ± 0.1 m/s. The top of a few adhered W grains was marked by focused ion beam (FIB), such marks can potentially verify grain rotation during remobilization.

Analysis of the samples has provided conclusive evidence of W dust remobilization, see figure 7. Let us briefly summarize our results: **(i)** Large W grains have a stronger remobilization tendency, but there is no sharp size cut-off. **(ii)** There are no appreciable remobilization activity differences between the sample that was exposed for a single discharge and the two samples that were exposed for multiple discharges. **(iii)** Very few tungsten grains were only displaced by plasma exposure without leaving the sample. Animations containing alternating SEM images of W samples prior to and post plasma exposure are provided in the online supplementary material.

4.3. Linear plasma device Pilot-PSI

Experimental set-up. A large number of experiments were carried out in Pilot-PSI, a linear plasma device capable of reproducing plasma conditions relevant for the divertor of ITER and future fusion devices [50, 51]. The optimized diagnostic access of Pilot-PSI allowed for camera observations of remobilized particles and estimates of their ejection velocities. A schematic drawing of Pilot-PSI and the camera arrangement is presented in figure 8. Two different set-ups were employed, see figure 9(a). In the perpendicular configuration, the samples were mounted on the target at the end of the plasma column, henceforth referred to as endplate, with the magnetic field lines normal to the sample surface. In the oblique configuration, the samples were mounted on an inclined plate inserted at the vicinity of the endplate, henceforth referred to as oblique plate, with

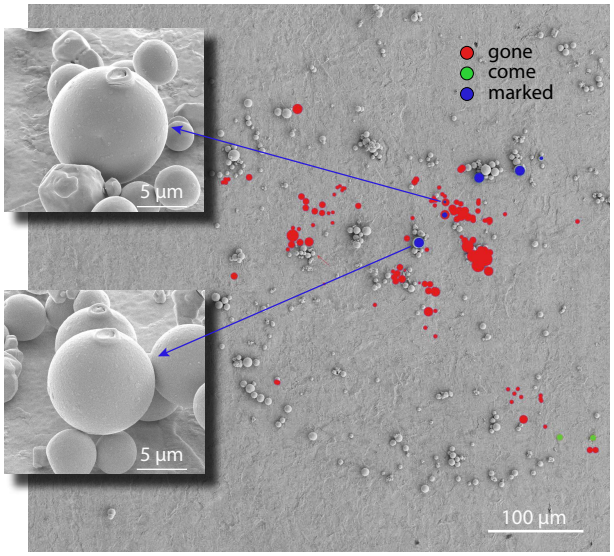

Figure 7. Synthesized secondary electron image of a tungsten dust spot before and after exposure to the EXTRAP-T2R plasma. The sample was exposed for multiple discharges. A large number of isolated grains and agglomerates was removed from the spot, two isolated grains were either displaced or originated from neighboring spots. The blue color indicates grains that were marked by FIB: the upper marked grains were removed, while the rest remained in their original position without exhibiting any signs of rotation.

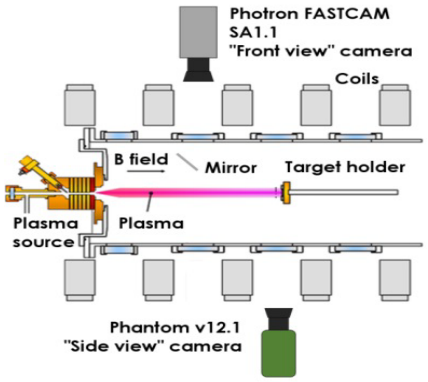

Figure 8. Top view of the Pilot-PSI device with the fast camera arrangement.

the magnetic field lines forming a 10° angle with the sample surface. The operating and plasma parameters varied: magnetic field $0.4-0.8\,\mathrm{T}$, discharge duration $1.5-2\,\mathrm{s}$, plasma current $180-220\,\mathrm{A}$, plasma density $(2-6)\times10^{20}\,\mathrm{m}^{-3}$ and electron temperature $0.4-1.1\,\mathrm{eV}$. These parameters refer to the plasma conditions at the endplate as measured by the Thomson scattering system. Such measurements could not be carried out for the oblique plate. Considering the geometry and size of the oblique obstacle but also plasma glow observations from the video data, we expect the local plasma to be more tenuous.

In these experiments, the W samples were disks of 30 mm diameter and 1 mm

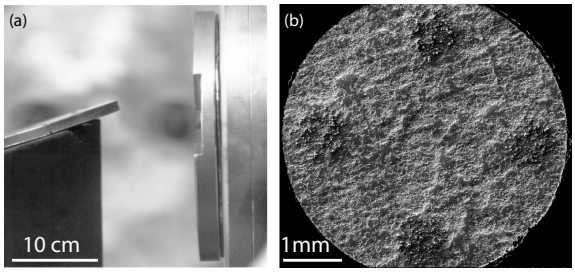

Figure 9. (a) The endplate and the oblique plate inside the Pilot-PSI vessel. (b) Secondary electron image of a dust spot set.

thickness. Each sample contains a single set of W dust spots, see figure 9(b). The set has a 2 mm diameter and lies at the center of the disk (which coincides with the center of the plasma column), in order to ensure dense local plasma given the radial decay of the plasma profiles within the column. It comprises of four symmetrically placed W dust spots of 0.5 mm diameter. The W grains are TEKMAT$^{\text{TM}}$ W-25 and were directly adhered to the W samples with impact velocities in the $0.6 - 1\,\text{m/s}$ range. The dust density in the spots was intentionally larger relative to the previous experiments in order to increase the number of trajectories observed by cameras and thus allow a reliable estimate of the characteristic ejection speed and angle.

Trajectories of remobilized W grains were recorded with the aid of two high-speed cameras. The configuration of viewing ports allowed us to have two views on the W sample, perpendicular to each other, thus allowing for a stereoscopic reconstruction of the dust trajectories. A Photron FASTCAM SA1.1 camera ("front view") was imaging the surface of the sample through a mirror installed inside the vacuum vessel, whereas a Phantom V12.1 camera ("side view") was observing the edge of the sample directly through the window. Both cameras were synchronized with the Pilot-PSI triggering system and had similar recording parameters: a frame rate of $5 - 10\,\text{kfps}$, a $1 - 20\,\mu\text{s}$ exposure time depending on the experimental conditions and a $\sim 200\,\mu\text{m/px}$ spatial resolution in the image plane. In addition, the "side view" camera was equipped with one Hα band-stop filter to filter out excessive plasma light emission in all the experiments, while the "front view" camera was equipped with a Hβ band-stop filter only in the oblique configuration (one filter of each kind was available for these experiments).

The dust grain trajectories were reconstructed using the TRACE code [52, 53]. The videos were pre-processed in order to remove the background plasma light and maximize dust visibility. After background subtraction, nearly all light stemming from the plasma was removed from the frame, except from the high-contrast sample - plasma interaction region. The residual plasma light was removed by subtracting an averaged image composed of 10 neighboring frames. These techniques also allowed us to increase the frame contrast in the vicinity of the glowing spots of adhered dust and therefore trace dust grains closer to the point of their remobilization.

Perpendicular configuration. Three samples were exposed to strong plasma ($n \sim 6 \times 10^{20}\,\text{m}^{-3}$ for $B = 0.8\,\text{T}$). Two of the samples exhibited very high remobilization

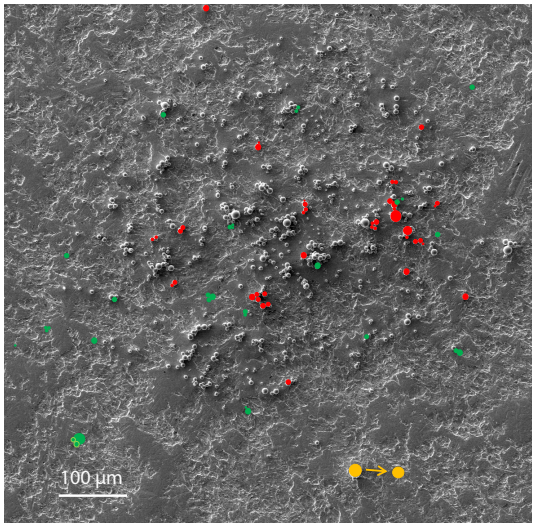

Figure 10. Synthesized secondary electron image of a tungsten dust spot before and after exposure to the Pilot-PSI plasma (perpendicular configuration, $n \sim 6\times10^{20}\,\mathrm{m}^{-3}$). A large number of grains were either removed or strongly displaced.

activity, the majority of dust was completely removed from the sample, while the remaining grains were strongly displaced destroying the circularity of the spots. Nearly all large grains have remobilized, whereas only a few of the smallest with size $\sim 5\,\mu$m remained at their original position. The third sample also exhibited high remobilization activity with many of the grains belonging at the larger side of the size distribution removed or strongly displaced (figure 10). Moreover, one of the samples that exhibited very high remobilization activity was re-exposed in identical plasma conditions. The re-exposure led to no additional remobilization. Finally, two samples were exposed to weaker plasma ($n \sim 2 \times 10^{20}\,\mathrm{m}^{-3}$ for $B = 0.4\,\mathrm{T}$), nearly none of the adhered grains remobilized. Animations containing alternating SEM images of W samples prior to and post plasma exposure are provided in the online supplementary material.

For the case of strong plasma, released grains were recorded by cameras and a number of trajectories was reconstructed enabling a calculation of the average velocity. The released W grains move nearly parallel to the endplate, at a distance of $0.4\pm0.2\,$mm with an average speed of $\sim 1.5\,$m/s. Typically, the initial observation point is a few millimeters away from the dust spot, owing to the strong relative brightness of background in the center of the plasma column.

Oblique configuration. Five samples were exposed to plasma with $B = 0.4 - 0.8\,\mathrm{T}$. As aforementioned, in this configuration, plasma is expected to be much weaker on the sample due to the large size / small inclination angle of the perturbing oblique plate. All samples exhibited very low remobilization activity, in some cases no grains were removed. In most of the spots, there are many instances where grains and small clusters were slightly displaced from their original position or rotated with respect to their contact area (figure 11). One of the samples was re-exposed in identical plasma conditions, the post and pre-exposure SEM images revealed no differences. Animations

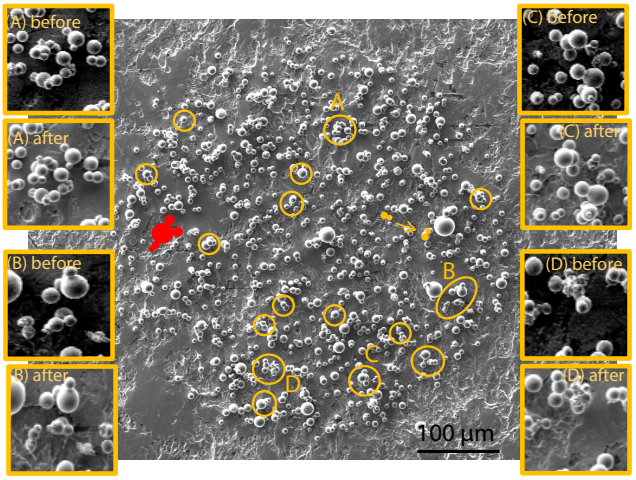

Figure 11. Synthesized secondary electron image of a tungsten dust spot before and after exposure to the Pilot-PSI plasma (oblique configuration). Only one W agglomerate was removed from the spot. The circled yellow regions indicate grains and clusters that were slightly displaced or weakly rotated.

containing alternating SEM images of W samples prior to and post plasma exposure are provided in the online supplementary material.

A number of trajectories was reconstructed by the camera observations. Some trajectories had an initial velocity component normal to the oblique plate, see figure 12(a), while most trajectories were initially nearly tangential to the oblique plate, see figure 12(b). The resolution is not sufficient to allow us to determine whether these grains are moving on the surface of the oblique plate or on the plasma sheath. Moreover, the grains become visible after the onset of remobilization, hence it is not possible to determine whether trajectories of the first type, initially had a purely tangential character.

5. Summary and conclusions

We stress again that the present studies refer exclusively to remobilization under normal operating plasma conditions, *i.e.* motion triggered by the action of plasma forces. The TEXTOR and EXTRAP-T2R experimental results confirmed that remobilization does take place under normal plasma operation and revealed that the condition for the grain release is not easily satisfied, since only a relative small fraction of the exposed populations has been remobilized and among those mostly larger grains and small clusters.

The interpretation of the Pilot-PSI data greatly benefits from being complemented by camera observations and from the multiple exposure of samples to identical plasma conditions. The experimental evidence from this device allow us to draw the following rather important conclusion: For a given "dust-PFC contact", there appears to be a condition to satisfy for remobilization to occur, in case it is not fulfilled in the beginning

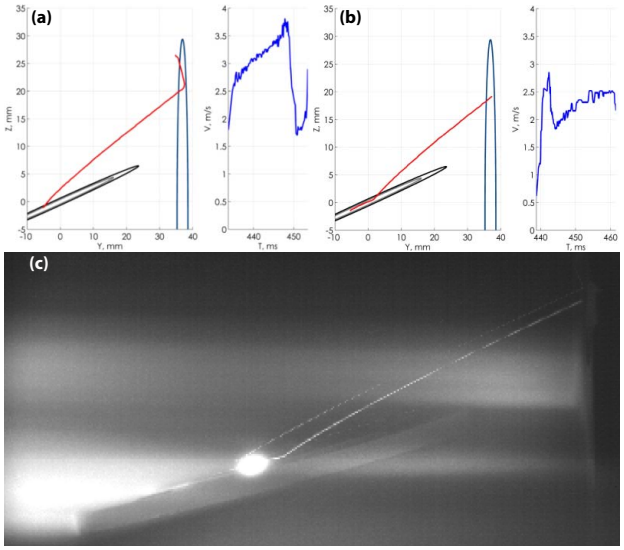

Figure 12. (a) Trajectory of remobilized W dust with an initial normal velocity component and calculated speed as a function of time. At the end of the trajectory the W grain impacts at the endplate. (b) Trajectory of remobilized W dust with a nearly tangential initial velocity and calculated speed profile as a function of time. (c) Superposition of frames from camera observations depicting the two trajectories. It is evident from the brightness of the column that the plasma is quenched on the beginning of the oblique plate, before reaching the sample (bright spot), which is mounted on the middle.

of the plasma exposure, then the grain shall remain adhered provided that the plasma conditions are stationary. Let us elaborate on this further. In Pilot-PSI the rise time of the magnetic field pulse is $\sim 1\,\mathrm{s}$, whereas the first plasma reaches the samples at $\sim 200\,\mathrm{ms}$. Subsequently, the plasma density gradually builds up to its maximum value which it attains at the plateau. According to the camera observations, dust remobilization events take place between 0.4 and 0.7 s of plasma exposure. Comparing SEM results with the number of observed released grains, we conclude that most of the events are resolved by the cameras, with the exception of the smallest or coldest released grains. This implies that even though it cannot be excluded that a few events in the very initial phase of the exposure are missed, we can confidently postulate that after a certain time no dust is released from the samples. This is strongly supported by the results of the re-exposure experiments. Namely, even samples with drastic remobilization activity upon their first exposure, did not exhibit a single incidence of remobilization after re-exposure to an identical discharge. This implies that, as the plasma profiles build up, once the plasma forces become strong enough to satisfy any of the three remobilization conditions for some of the grains, these grains are immediately displaced and further exposure to similar conditions will not lead to any additional activity.

Let us now view the theoretical estimates carried out in section 2 and the postulations about the three remobilization conditions in light of the experimental results. Our estimates of the pull-off force strength indicate that it is hard for

plasma forces along the surface normal to compensate for adhesion and that sliding or rolling can be realized easier than detachment. In fact, camera observations in the experiments reported here never revealed evidence of a direct lift-up. In the perpendicular configuration all grains moved radially along the sample surface, whereas in the oblique configuration the initial phase of trajectory was either pure tangential or with a dominant tangential component. Moreover, direct evidence of rolling / sliding have been obtained in a number of dust impact experiments on Pilot-PSI, for details see Ref.[18].

Overall, the experimental results are in line with the theoretical picture presented here. A quantitative analytical theory of remobilization is a formidable task. Self-consistent modelling of remobilization requires a consideration of the influence of dust on the local plasma parameters. Even for a single dust grain residing on the much larger PFC, while the global sheath structure will be unaffected, local effects will still be important owing to the strong dependence of the plasma forces on the micro-flows and details of the density profiles (sheath within a sheath case). Theoretical analysis can become even more complex for dust sizes comparable to the Debye length, for multiple grains due to shadowing effects or for castellated PFCs. However, the static nature of the phenomenon implies that particle-in-cell numerical modelling [54, 55] is a viable candidate that can provide quantitative results. Such investigations will be the subject of future work.

In view of such theoretical difficulties, controlled dust remobilization experiments in fusion environments are essential. The experimental technique proposed herein not only realistically mimics naturally occurring sticking impacts, but also allows for an unambiguous quantification of the dust remobilization activity.

Additional information

Animations containing alternating SEM images of W samples prior to and post plasma exposure allow for an evaluation of the remobilization activity without the use of synthesized images. Such animations are provided as supplementary information and available online.

Acknowledgments

Controlled pre-adhesion was made possible thanks to the engineering skills of Giambattista Daminelli. The authors would like to thank L. Frassinetti and H. Bergsåker for assistance in the experiments carried out on EXTRAP-T2R. P. T. would like to thank H. Bergsåker for bringing to his attention the issue of dust accumulation in gaps. This work has been carried out within the framework of the EUROfusion Consortium and has received funding from the European Unions Horizon 2020 research and innovation programme under grant agreement number 633053 (Enabling Research project CfP-WP14-ER-01/VR-01). The views and opinions expressed herein do not

necessarily reflect those of the European Commission.

References

[1] Bartels H.-W., Poucet A., Cambi G. *et al* 1998 *Fusion Eng. Des.* **42** 13
[2] Honda T., Bartels H.-W., Merrill B. *et al* 2000 *Fusion Eng. Des.* **47** 361
[3] Van Dorsselaere J. P., Perrault D., Barrachin M. *et al* 2009 *Fusion Eng. Des.* **84** 1905
[4] Humrickhouse P. W. and Sharpe J. P. 2008 *Fusion Eng. Des.* **83** 1721
[5] Gensdarmes F., Grisolia C., Roynette A. *et al* 2013 *Fusion Eng. Des.* **88** 2684
[6] Rudakov D. L., Yu J. H., Boedo J. A. *et al* 2008 *Rev. Sci. Instrum.* **79** 10F303
[7] Rudakov D. L., Litnovsky A., West W. P. *et al* 2009 *Nucl. Fusion* **49** 085022
[8] Rohde V., Balden M., Lunt T. *et al* 2009 *Phys. Scr.* **T138** 014024
[9] De Temmerman G., Bacharis M., Dowling J. and Lisgo S. 2010 *Nucl. Fusion* **50** 105012
[10] Roche H., Barbuti A, Bucalossi J. *et al* 2011 *Phys. Scr.* **T145** 014022
[11] Giovannozzi E., Beurskens M., Kempenaars M. *et al* 2010 *Rev. Sci. Instrum.* **81** 10E131
[12] Martynenko Yu. V. and Nagel M. Yu. 2012 *Plasma Phys. Rep.* **38** 290
[13] Coenen J. W., Sertoli M., Brezinsek S. *et al* 2013 *Nucl. Fusion* **53** 073043
[14] Sertoli M., Flannegan J. C., Cackett A. *et al* 2014 *Phys. Scr.* **T159** 014014
[15] Flanagan J. C., Sertoli M., Bacharis M. *et al* 2015 *Plasma Phys. Control. Fusion* **57** 014037
[16] Ratynskaia S., Vignitchouk L., Tolias P. *et al* 2013 *Nucl. Fusion* **53** 123002
[17] Vignitchouk L., Tolias P. and Ratynskaia S. 2014 *Plasma Phys. Control. Fusion* **56** 095005
[18] Ratynskaia S., Tolias P., Shalpegin A. *et al* 2014 *J. Nucl. Mater.* http://dx.doi.org/10.1016/j.jnucmat.2014.09.064
[19] Ribeiro I., Damiani C., Tesini A. *et al* 2011 *Fusion Eng. Des.* **86** 471
[20] Pitts R. A., Carpentier S., Escourbiac F. *et al* 2013 *J. Nucl. Mater.* **438** S48
[21] Carpentier-Chouchana S., Hirai T., Escourbiac F. *et al* 2014 *Phys. Scr.* **T159** 014002
[22] Tomita Y. *et al* 2006 *Contrib. Plasma Phys.* **46** 617
[23] Tomita Y. *et al* 2007 *J. Nucl. Mater.* **363-365** 264
[24] Tomita Y. *et al* 2009 *J. Nucl. Mater.* **390-391** 164
[25] Ueno M. *et al* 2012 *Contrib. Plasma Phys.* **52** 478
[26] Stronge W. J. 2000 *Impact Mechanics* (Cambridge: Cambridge University Press)
[27] Thornton C. and Ning Z. 1998 *Powder Technol.* **99** 154
[28] Krijt S., Güttler C., Heißelmann D. *et al* 2013 *J. Phys. D: Appl. Phys.* **46** 435303
[29] Johnson K. L., Kendall K. and Roberts A. D. 1971 *Proc. R. Soc. Lond. A* **324** 301
[30] Barthel E. 2008 *J. Phys. D: Appl. Phys.* **41** 163001
[31] Greenwood J. A. 2009 *Phil. Mag.* **89** 945
[32] Derjaguin B., Muller V. M. and Toporov Yu. P. 1975 *J. Colloid Interface Sci.* **53** 314
[33] Israelachvili J. N. 2011 *Intermolecular and surface forces* (New York: Academic Press)
[34] Visser J. 1995 *Particul. Sci. Technol.* **13** 169
[35] Hutchinson I. H. 2006 *Plasma Phys. Control. Fusion* **48** 185
[36] Lebedev N. N. and Skal'skaya I. P. 1962 *Soviet Phys. Tech. Phys.* **7** 268
[37] Tabor D. 1977 *J. Colloid Interface Sci.* **58** 2
[38] O'Neill M. 1968 *Chem. Eng. Sci.* **23** 1293
[39] Sharma M. M. *et al* 1992 *J. Colloid Interface Sci.* **149** 121
[40] Popov V. L. 2010 *Contact mechanics and friction: physical principles and applications* (Berlin: Springer-Verlag)
[41] Rabinowicz E. 1995 *Friction and wear of materials* (New York: John Wiley & Sons)
[42] Tabor D. 1981 *ASME J. Lubr. Technol.* **103** 169
[43] Müser M. H., Wenning L. and Robbins M. O. 2001 *Phys. Rev. Lett.* **86** 1295
[44] Hubbe M. A. 1984 *Colloids Surf.* **12** 151
[45] Soltani M. and Ahmadi G. 1994 *J. Adhesion Sci. Technol.* **8** 763

[46] Burdick G. M., Berman N. S. and Beaudoin S. P. 2001 *J. Nanopart. Res.* **3** 455
[47] Burdick G. M., Berman N. S. and Beaudoin S. P. 2005 *Thin Solid Films* **488** 116
[48] Brunsell P., Bergsåker H., Cecconello M. *et al* 2001 *Plasma Phys. Control. Fusion* **43** 1457
[49] Bykov I., Vignitchouk L., Ratynskaia S. *et al* 2014 *Plasma Phys. Control. Fusion* **56** 035014
[50] van Rooij G. J., Veremiyenko V. P., Goedheer W. J. *et al* 2007 *Appl. Phys. Lett.* **90** 121501
[51] De Temmerman G., Zielinski J. J., van Diepen S. *et al* 2011 *Nucl. Fusion* **51** 073008
[52] Zayachuk Y., Brochard F., Bardin S. *et al* 2010 arXiv:1010.3432v1
[53] Endstrasser N., Brochard F., Rohde V. *et al* 2011 *J. Nucl. Mater.* **415** S1085-S1088
[54] Komm M., Dejarnac R., Gunn J. P. and Pekarek Z. 2013 *Plasma Phys. Control. Fusion* **55** 025006
[55] Delzanno G. L., Camporeale E., Moulton J. D., Borovsky J. E., MacDonald E. A. and Thomsen M. F. 2013 *IEEE Trans. Plasma Sci.* **41** 3577